Developing Tools for Assessing Bend-twist Coupled Foils

Laura Marimon Giovannetti, Joseph Banks, Stephen R. Turnock, Stephen W. Boyd,
University of Southampton, Southampton/UK, L.Marimon-Giovannetti@soton.ac.uk

1 Introduction

For many applications, the ability of a foil to passively adapt to the experienced fluid loading could be advantageous, Nicholls-Lee & Turnock (2007): e.g. wind or tidal turbine blades, hydrofoils for sailing yachts, or marine propellers. Composite materials provide the opportunity to tailor the bend twist coupling of a structure to achieve these goals, Veers & Bir (1998). To allow such foils to be designed and assessed, numerical tools such as finite element analysis (FEA) and computational fluid dynamics (CFD) will need to be coupled together in fluid-structure interaction (FSI) simulations. Currently, there is a lack of experimental validation data for FSI investigations. This paper details experiments conducted on a flexible NACA0015 foil.

2 Experimental Data

The experiments were conducted in the 3.5 m x 2.4 m RJ Mitchell wind tunnel at the University of Southampton, Fig.1. This closed circuit tunnel operates at wind speeds of 4 to 40 m/s with less than 0.2% turbulence. A six-component Nutem load cell balance is mounted on a turntable in the tunnel roof. This allows forces and moments to be measured in the turntable axis system about the balance centre 1.27 m below the tunnel roof. The aluminium beam protruding from the foil is attached to the overhead balance using a rigid clamping structure.

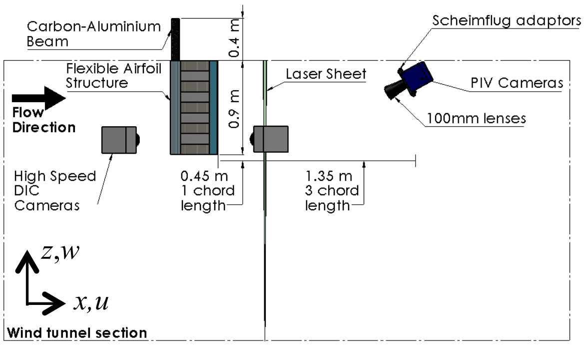

Fig.1: Schematic of experimental set up

Digital Image Correlation (DIC), Giovannetti et al. (2014), measured the full field deflection at the board tip. Particle Image Velocimetry (PIV) captured the position and strength of the tip vortex. Preliminary FSI simulations are compared to this data. Fig.2 shows the investigated NACA0015 foil.

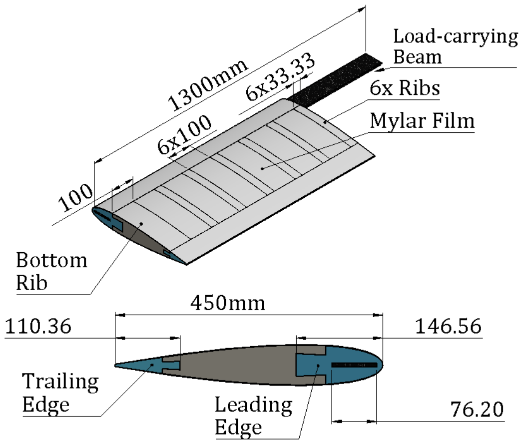

Fig.2: Tested foil design

The forces were measured at 1kHz and converted into the tunnel axis system to provide sideways lift coefficient (C_L), vertical force coefficient (C_Z) and drag coefficient (C_D).

A stereo DIC system was set up in the wind tunnel allowing 3D deflection data to be captured within a 0.5x0.5m field of view at the board tip. Fig.3 shows the DIC and PIV systems working simultaneously in the wind tunnel.

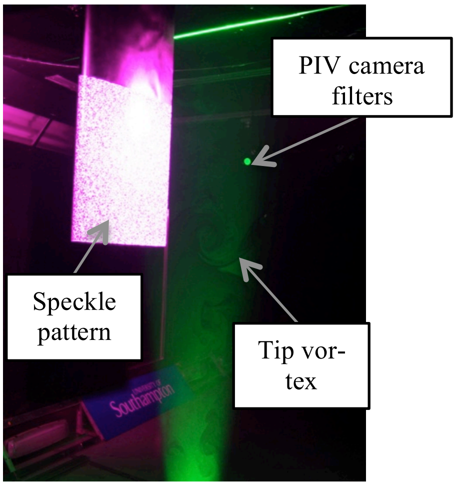

Fig.3: DIC and stereo-PIV set up

2.1 Flow field measurement

A PIV laser sheet was set up one chord (0.45m) behind the trailing edge of the foil and perpendicular to the flow direction. Two 29 MP cameras were positioned behind the board tip, with a 100mm Nikon lens providing a 0.4x0.11m area of interest. Seeding particles were introduced into the tunnel using a smoke machine on a timer. The time between the two image frames was set to ensure that most particles were observed in both frames. Then a series of 120 pairs of images were taken at a constant frame rate of 2Hz.

The angle of attack was set to 15°, and a range of wind tunnel speeds were tested. The images were processed using the LaVision software DaVis.

3 Numerical Simulations

A numerical model of the generic aerofoil structured tested in the wind tunnel is developed. The aim is to provide a numerical prediction of this structure to fluid loading validated with experiments. The numerical analysis has been approached systematically, firstly assessing the validity of the FEA model from a simple beam, building the geometry complexity to its final shape, containing the foam-rib structure as well as the Mylar sheet. Moreover, the coupling scheme between FEA and CFD solvers was investigated. The software used are ABAQUS 6.13 for the structural solver and Star-CCM+ 8.04 for the fluid solver.

In an FSI simulation, such as the one encountered, the sets of differential equations and boundary conditions associated with the fluid and structure domains must be satisfied simultaneously. The two domains are interconnected using the SIMULIA Co-simulation Engine (CSE) through a common physical interface surface that comprises of the aerofoil and 50 mm of the load-carrying beam, as in the wind tunnel experiments. In the co-simulation the nodal displacements are exported in the global coordinate systems from the FEA solver and the pressure normal to the element surfaces are imported back in the CFD environment.

3.1 Finite Element Analysis domain

In order to correctly reproduce the tested geometry in ABAQUS 6.13 it was necessary to model accurately the contact surfaces, joining them so that there was no relative motion between them.

Solid second order elements were chosen to represent the load-carrying beam as well as the foam structures and quadratic shell element were used to represent the Mylar sheet. Second-order element were chosen to avoid shear locking (i.e. occurring to first order elements subject to bending where parasitic shear are created) and hourglassing effects (i.e. occurring to first-order reduced integration elements in stress-displacement studies where the strains calculated at the integration points results as being zero).

The load-carrying beam was modelled as a solid composite section with one element through thickness as in composite sections each element contains the number of plies defined in the section (ABAQUS Simulia, 2013). In order to increase the accuracy of the results for the calculation of stresses and strains the number of integration points is increased to 21. This allows a smooth stress and strain distribution to be captured for each ply in the through thickness direction. Fig.4 shows the load-carrying beam with the aluminium section in the core, the two carbon plies as skin elements and the 21 integration points (i.e. blue dots within each material).

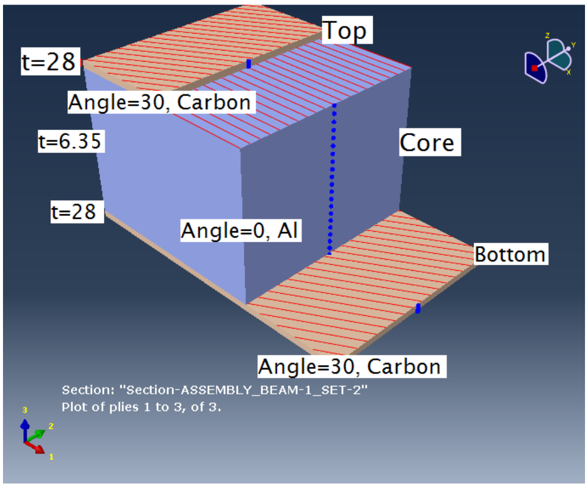

Fig.4: Composite beam structure representation for a ply angle of 30°.

Each element of the flexible aerofoil is meshed separately but consistency in nodes position was assessed, constraining the mesh size at the boundaries between each different structural element, so to ensure that the same number of nodes was kept at the interfaces.

Fig.5 shows a view of the complete wind tunnel geometry represented in ABAQUS. The boundary conditions set in the FEA environment replicate the ones encountered in the wind tunnel, fixing in translation and rotation the first 350 mm of the load-carrying beam. This region is therefore not modelled in the CFD as it is out-side the domain walls.

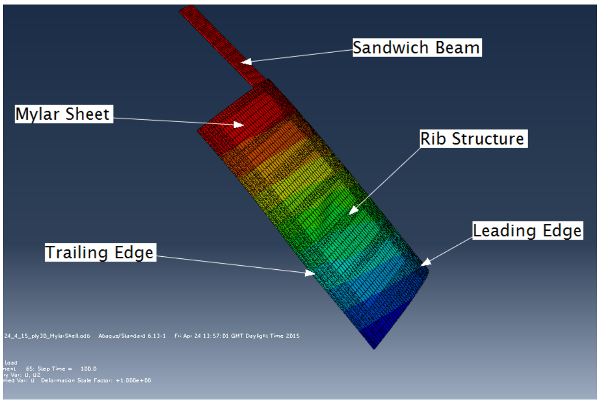

Fig.5: FEA structure comprising of the load-carrying beam, the foam and the Mylar structures

Table 1 shows the material properties used in the FEA model. The carbon and foam properties are anisotropic and aluminium and Mylar are considered isotropic materials.

Table 1: Material properties used in FEA model

Material	Property	Value
Aluminium	ρ	2.7 e^{-9} tonne mm^{-3}
	E	55000 MPa
	ν	0.35
Carbon	ρ	3 e^{-9} tonne mm^{-3}
	E_1	117940 MPa
	E_2	7840 MPa
	E_3	7840 MPa
	ν	0.25
	G_{12}	4400 MPa
	G_{13}	3600 MPa
	G_{23}	4400 MPa
Foam	ρ	3.6 e^{-12} tonne mm^{-3}
	E_1	10.4 MPa
	E_2	10.4 MPa
	E_3	10.4 MPa
	ν	0.3
	G_{12}	10.14 MPa
	G_{13}	10.14 MPa
	G_{23}	10.14 MPa
Mylar	ρ	1.39 e^{-9} tonne mm^{-3}
	E	283.509 MPa
	ν	0.35

3.2 CFD domain

We used the finite-volume RANSE solver Star-CCM+ 8.0.4 with the k-ω SST turbulence model. A dynamic implicit solution is chosen given the strong physical coupling deriving from the highly flexible specimen. In the implicit iterative approach the fields are exchanged multiple times per coupling step until an overall equilibrium is achieved prior to advancing to the next coupling step. The coupling step size need to be specified in the two solvers and define the period between the two consecutive exchanges, therefore the frequency of exchange between the analyses. Using a constant coupling size allows both analyses to advance while exchanging data at set target points according to:

$$t_{i+1} = t_i + \Delta t_c \qquad 3\text{-}1)$$

Δt_c is a value that defines the coupling step size to be used through the coupled simulation, t_{i+1} is the target time and t_1 is the time at the start of the coupling step, here 0.0025 s in both solvers.

The fluid domain was set as a box-section 10.7x3.5x2.4 m replicating the wind tunnel dimensions to correctly capture the fluid behaviour. The aerofoil was positioned 4 m downstream of the inlet, attached to the domain roof and centred in the cross-domain direction, as in the working section during the experiments.

The trimmer mesh with mesh morpher scheme was selected to allow the mesh to follow the nodal displacement given by the solid solver. Twelve prism layers were set along the aerofoil; the first prism layer thickness was set to y=6.55x10^{-4}m assuming y^+=50 for a base wind speed V_S=25 m/s. Mesh refinement regions were set around the aerofoil, especially around the leading edge, the root and tip as well as the root and tip vortices regions, Fig.6. The final mesh of the fluid domain had 2,500,000 cells.

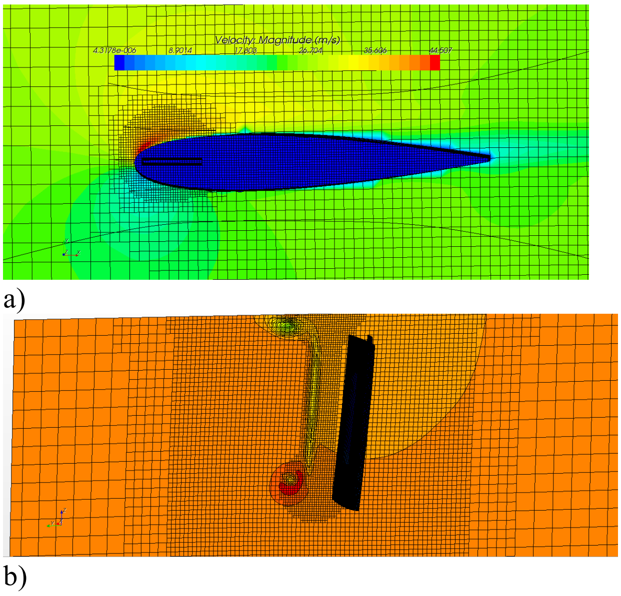

b)

Fig.6: Mesh around the aerofoil and at a plane 1 chord downstream of the trailing edge - PIV laser sheet position.

4 Experimental Results

Fig.7 presents the results for the aerofoil tip deflection in the wind tunnel at different wind speeds for a steady angle of attack of 15°. Note the small discrepancies in measures for DIC-only runs and coupled DIC-PIV runs.

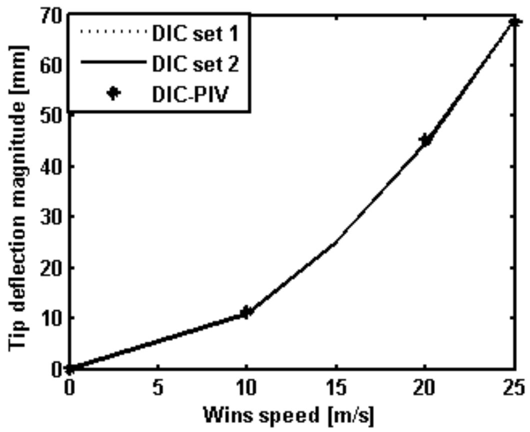

Fig.7: Tip deflection measured with DIC at different wind speeds

4.1 Flow field

The basic VORTFIND algorithm, Pemberton et al. (2002), was used to locate the centre of the tip vortex in the 120 vector fields produced for each experimental configuration. The algorithm finds the in-plane vectors closest to a vortex centre using criteria defined in Phillips & Turnock (2013). The average position of the 10 closest vectors was then taken as the vortex position for each vector field.

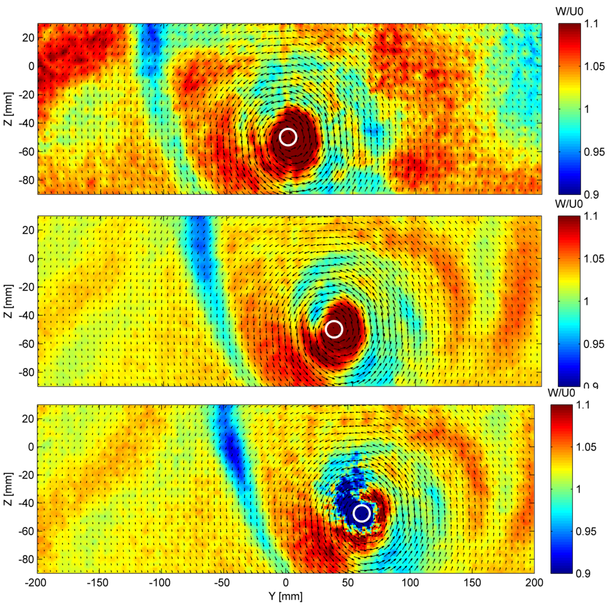

Fig.8: Time averaged axial velocity distribution relative to the free stream velocities: 10, 20 and 25 m/s (from top to bottom). The in-plane velocity field is represented as vectors. The vortex centre calculated from the mean velocity field is represented by a white circle.

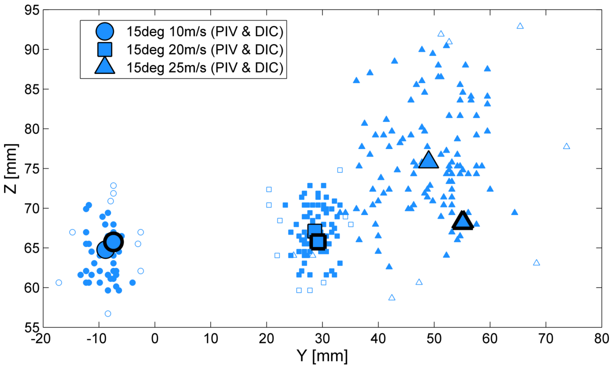

Fig.9: Instantaneous vortex positions from 120 images in-plane vector fields for different free stream velocities. The mean value of these positions is indicated by a large marker with a thin boarder. The vortex position obtained from the time averaged velocity field is indicated by a large marker with a bold border.

5 Numerical Results

The first five modes natural frequencies were initially investigated in FEA. Results were validated against impact tests performed on the wind tunnel structure, Table 2, showing good agreement. This allowed assessing the validity of the material properties selected in the FEA simulations.

Table 2: First five mode natural frequencies of the flexible aerofoil in experiments and FEA

Mode number	Numerical	Experimental
1	4.20 Hz	4.44 Hz
2	15.21 Hz	15 Hz
3	30.03 Hz	24.99 Hz
4	34.18 Hz	35 Hz
5	41.74 Hz	45 Hz

In order to build confidence on the FEA model, the structure was tested initially with different geometries (i.e. foam as a full-solid section, the foam as a rib-structure without the Mylar sheet and finally the whole wind tunnel model). Furthermore the initial load was applied at the centre of effort location and then a constant pressure load was applied to the FEA surface. Fig.11 compares experiments and initial FEA. Note how the tip displacement increases for the only-rib structure. The results obtained with the final FEA model (i.e. Mylar structure) are very close to the ones measured with DIC. Fig.12 compares qualitatively between the DIC, FEA only and coupled FSI displacements. Note how the aerofoil experiences higher deflections near the tip and toward the trailing edge, as expected.

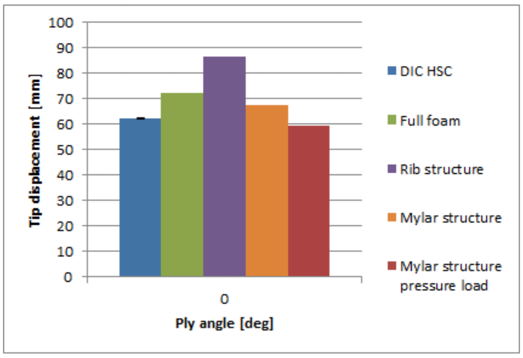

Fig.10: Tip displacement comparison between DIC and different FEA configurations

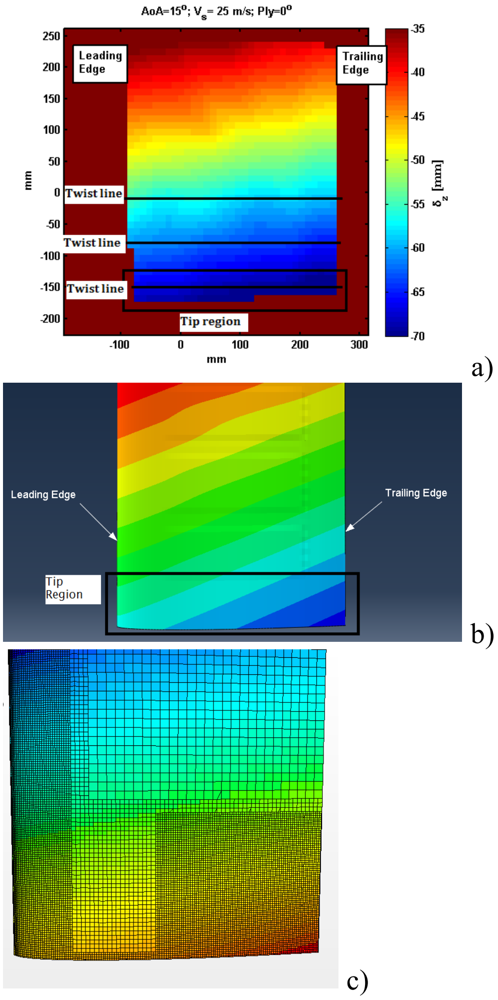

Fig.11: DIC, FEA and FSI out-of-plane displacements for AoA=15° and Vs=25 m/s (scale 30-80 mm)

Fig.12a shows the axial velocity at a plane one chord downstream of the trailing edge (the location of the laser sheet in the PIV experiments). Note the deflected aerofoil in the CFD environment.

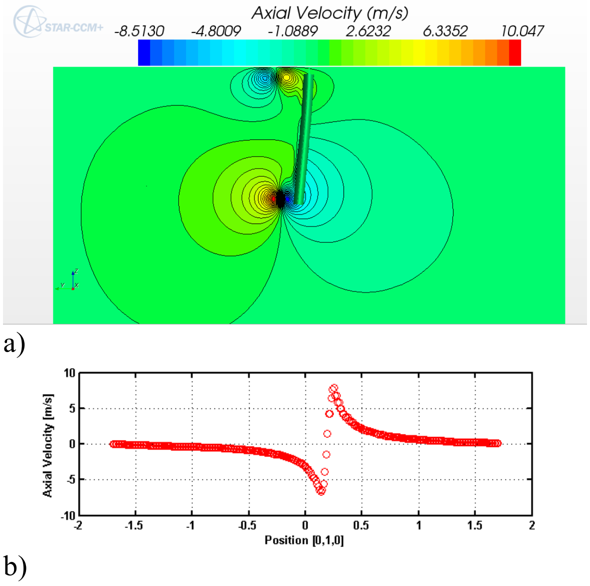

Fig.12: Axial velocity at a plane one-chord downstream of the aerofoil

Fig.12b shows that the tip vortex is located at the maximum axial velocity perturbation, where the free-stream velocity changes with a maximum at the vortex centre location.

Acknowledgements

We would like to thank the help of the TSRL team, Dave Hollis from LaVision, the RJ Mitchell wind tunnel staff and the research funding from the EPSRC (grant number EP/009876/1).

References

Giovannetti, L. M., Banks, J., Soubeyran, X., Turnock, S. R., & Boyd, S. W. (2014). Full-field deformation response of a high performance foil under fluid loading using Digital Image Correlation. *Ready for submission*.

Nicholls-Lee, R. F., & Turnock, S. R. (2007). Enhancing Performance of a Horizontal Axis Tidal Turbine using Adaptive Blades. In *OCEANS 2007 - Europe* (pp. 1–6). Aberdeen: Ieee. doi:10.1109/OCEANSE.2007.4302437

Veers, P.; Bir, G. (1998). Aeroelastic tailoring in wind-turbine blade applications. *Windpower'98,* *American Wind Energy Association Meeting and Exhibition*. Bakersfield, California. http://windpower.sandia.gov/other/AWEA4-98.pdf

Pemberton, R.; Turnock S.; Dodd, T.R.E. (2002). A novel method for identifying vortical structures. *J. Fluids and Structures*, *16*(23), 1051–1057.

Phillips, A., Turnock, S. (2013). Application of the VORTFIND algorithm for the identification of vortical flow features around complex three-dimensional geometries. *Int. J. for Numerical Methods in Fluids*, *71*(11), 1461–1474. doi:10.1002/fld.3720